Erschienen in: Journal of Physics : Condensed Matter ; 30 (2018), 2. - 024003
https://dx.doi.org/10.1088/1361-648X/aa9de4

Elastic moduli of a Brownian colloidal glass former

S Fritschi and M Fuchs

Fachbereich Physik, Universität Konstanz, 78457 Konstanz, Germany

E-mail: sebastian.fritschi@uni.kn

Abstract

The static, dynamic and flow-dependent shear moduli of a binary mixture of Brownian hard disks are studied by an event-driven molecular dynamics simulation. Thereby, the emergence of rigidity close to the glass transition encoded in the static shear modulus G_∞ is accessed by three methods. Results from shear stress auto-correlation functions, elastic dispersion relations, and the elastic response to strain deformations upon the start-up of shear flow are compared. This enables one to sample the time-dependent shear modulus $G(t)$ consistently over several decades in time. By that a very precise specification of the glass transition point and of G_∞ is feasible. Predictions by mode coupling theory of a finite shear modulus at the glass transition, of α-scaling in fluid states close to the transition, and of shear induced decay in yielding glass states are tested and broadly verified.

Keywords: shear modulus, glass transition, Brownian dynamics simulation, rheology, colloidal dispersion, dispersion relation

1. Introduction

The rheology of colloidal glass-forming dispersions is of broad interest. On the one hand, the flow properties of dense dispersions play a crucial role in many technological applications [1], on the other hand colloidal solutions have become a model system for the investigation of the glass transition [2]. A dispersion of slightly polydisperse colloidal hard spheres vitirifies upon densification without undergoing crystal nucleation [3], and its rheology has been analyzed using concepts describing glassy arrest [4, 5]. Adding colloids to the solution up to a finite concentration, the dispersion first becomes a viscoelastic liquid with (Newtonian) viscosity far exceeding the one of the pure solvent. Increasing the concentration beyond a critical value the liquid transforms into an amorphous solid accompanied by the emergence of mechanical rigidity to shear deformations on laboratory time scales. The density dependent macroscopic viscoelastic properties can be quantified in terms of the time-dependent shear modulus, which contains Brownian, hydrodynamic and potential contributions [1, 6]. The emergence of mechanical rigidity at the colloidal glass transition has widely been related to the contributions arising from the direct potential interactions among the particles [2]; for a differing view see [7]. Thereby investigations on colloidal systems can be related to theoretical investigations or molecular dynamics simulations which aim for a microscopic understanding of universal shear stress correlations at the glass transition [8–17].

The mode coupling theory (MCT) of structural relaxation in liquids explains viscoelasticity in fluids and the emergence of elasticity at the glass transition [18]. It provides explicit results for the potential part of the time-dependent shear modulus $G(t)$ in fluids of hard spheres [19–22], which have quantitatively been compared to colloid data [4, 23]. The theory has been generalized to the nonlinear rheological response for arbitrary homogeneous flow rates [24, 25], which also has been compared to rheology data from colloidal dispersions [5, 23, 26]. The central quantity of MCT capturing the shear elasticity is the static shear modulus G_∞ [18], which e.g. determines the transverse sound velocity in molecular glasses. In overdamped systems, like colloidal dispersions or Brownian particle systems, it determines (i) the plateau at intermediate times of the shear stress correlation function in fluid states, or (ii) its long-time limit in (ideal) glass states. In rheological

experiments, it appears as a plateau in the linear storage modulus $G'(\omega)$ for low frequencies [5]. This plateau extends to arbitrarily low frequencies in ideal glass states (case (ii) above; but see [27] for deviations in nonideal glass states).

The present contribution explores by computer simulations different strategies to determine the static shear modulus G_∞ of a Brownian particle system close to its ideal MCT glass transition. The aim of our work is to test the MCT prediction, that a unique G_∞ exists which can be observed by different measurements. Also, we aim to determine its dependence on the thermodynamic control parameters. A well studied binary mixture of hard disks [28–32] moving in two dimensions ($d = 2$) is chosen as simple model system where stress fluctuations at long times can be sampled efficiently. Fixing the size ratio and the concentrations, the packing fraction ϕ, viz. the fraction of the area filled by the disks, is the only control parameter. The shear modulus $G_\infty(\phi)$ close to the glass transition at ϕ_c is determined using three different simulation protocols. (I) The plateau values of the shear stress auto-correlation function, (II) the dispersion relations obtained from static displacement fluctuations, and (III) the system's linear response to strain deformations upon the start-up of simple shear flow are determined. Comparing the mechanical properties seen via these three strategies provides insights into the vitrification process and the transition from viscous to emergent elastic response.

The paper is organized as follows: first the theoretical basis provided by the combination of an integration-through transients (ITT) approach to nonlinear response with the mode-coupling theory of the glass transition (MCT) is recalled, on how to measure the static shear modulus G_∞ in glass-forming systems of Brownian particles. This suggests three methods for computer simulations, which are described in section 3. Using an event driven algorithm, shear-stress auto-correlation functions, transversal dispersion relations, and stress–strain relations in start-up shear flow are presented and studied in a two-dimensional binary mixture of hard disks. In section 4, the different results for $G(t)$ and G_∞ are discussed. Conclusions end the manuscript.

2. Theory

For quiescent liquids, MCT predicts the existence of an ideal glass transition [18], which rationalizes many findings in colloidal dispersions [2, 33–36]. It arises from a feedback mechanism in the coupling of local structural correlations ('cage effect'), and leads to transient particle localization and shear rigidity. The MCT for quiescent liquids has been generalized to homogeneously flowing systems considering colloidal glass formers [24, 25]. Flow introduces the effect of the (affine) advection of long-wavelength fluctuations to short wavelengths. This causes a flow-induced breaking of cages and melting of glass. The history of the competition of both dynamical mechanisms enters via integrating through the transients (ITT) even in cases where stationary states are considered. Predictions of ITT-MCT have been compared to experiments on model colloidal suspensions and found to provide a semi-quantitative description of many flow properties, including shear-thinning of the supercooled liquid and plastic flow or dynamic yielding of the glass [5, 26, 34–36]. Comparisons with computer simulations also verified many of the predictions [37–39], as well as did event driven simulations of the chosen Brownian particle mixture [28–32]. We extend the tests of ITT-MCT by BD simulations by studying three different quantities simultaneously in order to test whether G_∞ is a well defined material parameter as predicted.

2.1. Stress response

The rheological response of a fluid of Brownian particles to homogeneous but otherwise arbitrary incompressible flows is given by a generalized Green–Kubo relation [24, 25]

$$\boldsymbol{\sigma}(t) = \frac{V}{k_\mathrm{B}T}\int_{-\infty}^{t} \mathrm{d}t_1\, \langle \boldsymbol{\kappa}(t_1) : \hat{\boldsymbol{\sigma}}\, e_-^{\int_{t_1}^{t} \mathrm{d}s\, \Omega^\dagger(s)}\hat{\boldsymbol{\sigma}}\rangle^{\mathrm{eq}}. \qquad (1)$$

Here, $\hat{\boldsymbol{\sigma}}$ is the fluctuating stress tensor depending on the instantaneous particle positions and $\boldsymbol{\sigma}$ its macroscopic average. Brackets denote canonical averaging, and e_- the negatively time-ordered matrix exponential. V is the volume and $k_\mathrm{B}T$ thermal energy. The flow velocity gradient is denoted as $\boldsymbol{\kappa}(t) = (\nabla \mathbf{v})^T$. It is homogeneous and traceless, $\boldsymbol{\kappa} : \mathbf{1} = 0$, in order to describe incompressible flow of the featureless background relative to which the particles perform random walks. The distribution function of the particles obeys Smoluchowski's equation containing the time evolution operator $\Omega(t)$. Neglecting the flow-dependence of the time-evolution operator leads to the linear response result

$$\begin{aligned}\boldsymbol{\sigma}^{\text{lin resp}}(t) &= \frac{2V}{k_\mathrm{B}T}\int_{-\infty}^{t} \mathrm{d}t_1\, \langle \hat{\sigma}_{xy}\, e_-^{\Omega_{\mathrm{eq}}^\dagger (t-t_1)}\hat{\sigma}_{xy}\rangle^{\mathrm{eq}}\, \bar{\boldsymbol{\kappa}}(t_1)\\ &= 2\int_{-\infty}^{t} \mathrm{d}t_1\, G(t-t_1)\, \bar{\boldsymbol{\kappa}}(t_1). \qquad (2)\end{aligned}$$

Here, we used that only one response function, the time-dependent shear modulus $G(t)$, arises for incompressible flow and that the microscopic stress tensor is symmetric [25, 40]. Thus, only the symmetrized velocity gradient enters $\bar{\boldsymbol{\kappa}} = (\boldsymbol{\kappa} + \boldsymbol{\kappa}^T)/2$. Equation (2) defines the linear shear modulus $G(t)$.

In the general flow case, not only the transversal (or shear) modulus appears but also the longitudinal one [31, 41, 42]:

$$\mathbf{G}(\mathbf{q}, t) = \hat{\mathbf{q}}\hat{\mathbf{q}}\, G_q^{\parallel}(t) + (\mathbf{1} - \hat{\mathbf{q}}\hat{\mathbf{q}})\, G_q(t). \qquad (3)$$

Here, we stated the generalization of the stress memory kernel to finite wavevector $\mathbf{q}$ (with $\hat{\mathbf{q}} = \mathbf{q}/q$ denoting its direction); it will be used in the next section. We assume that the macroscopic shear modulus $G(t)$ is obtained in the long wavelength limit, $G(t) = \lim_{q\to 0} G_q(t)$; but see [43] for a discussion that this limit is actually non-analytic.

In the rheological investigations, we will consider the special case of simple shear flow in x-direction, varying linearly in y-direction: ($\kappa_{\alpha\beta}(t) = \dot{\gamma}(t)\delta_{x\alpha}\delta_{y\beta}$, where $\dot{\gamma}(t)$ is the shear rate). The shear stress at finite shear rates is then given by

$$\sigma_{xy}(t) = \int_{-\infty}^{t} \mathrm{d}t_1\, \dot{\gamma}(t_1)\, G(t, t_1; [\dot{\gamma}]), \qquad (4)$$

which serves to define the nonlinear shear modulus, $G(t, t_1; [\dot\gamma])$. It is a functional of the velocity gradient tensor, and generalizes the linear modulus defined in equation (2) to finite shear rates.

2.2. Strain fluctuations

Displacement fluctuations at the glass transition have recently been of interest because they reveal intriguing far-field correlations [44]. These originate from force correlations in metastable solids and provide an alternative venue to access elastic correlations [42, 45]. In an idealized glass state, the long-time limit of the linear moduli is finite: $\mathbf{G}_\infty(\mathbf{q}) = \mathbf{G}(\mathbf{q}, t \to \infty)$. Obtaining collective displacement fluctuations $\mathbf{u}_\mathbf{q}(t)$ from integrating up velocity fluctuation, viz. solving $\dot{\boldsymbol{u}}_q(t) = \mathbf{v}_\mathbf{q}(t)$, MCT predicts an equipartition theorem for static displacement correlations in glass [42]:

$$(\langle \mathbf{u}_\mathbf{q}{}^* \mathbf{u}_\mathbf{q} \rangle^{\text{glass}})^{-1} = \frac{q^2}{n k_\text{B} T} \left(\mathbf{G}_\infty(\mathbf{q}) + \frac{\hat{\boldsymbol{q}}\hat{q}}{\kappa_q^T} \right) = \frac{\mathcal{D}(\mathbf{q})}{k_\text{B} T}. \tag{5}$$

The equal time displacement variance, averaged over a restricted phase space associated with the glassy state, is determined by the tensor of elastic coefficients $\mathbf{G}_\infty(\mathbf{q})$. The long range of displacement correlations arises from the $1/q^2$ variation in equation (5) for small q. In equation (5), κ_q^T is the isothermal compressibility (of the underlying fluid state generalized to finite q), n the number density and $\mathcal{D}$ stands for the dynamical matrix studied to obtain insight into the elastic spectrum of the system [45]. Its eigenvalues $\lambda_\parallel(q)$ and $\lambda_\perp(q)$ represent the longitudinal and parallel dispersion relation and are related to the Lamé coefficients μ and λ in the long wavelength limit [46]; see below.

2.3. ITT-MCT stability analysis of glassy structure

The theoretical results summarized in the previous two subsections contain various limits of a nonlinear, wavevector- and time- dependent shear memory kernel $G(t, t_1, \mathbf{q}; [\dot\gamma])$. In the quiescent system, $G_q(t - t_1) = G(t, t_1, \mathbf{q}; [\dot\gamma = 0])$, and under steady homogeneous flow, $G(t, t_1; [\dot\gamma]) = G(t, t_1, \mathbf{q} = \mathbf{0}; [\dot\gamma])$. The crucial ITT-MCT prediction which we will test in the following is the nonlinear stability relation, first considered by Götze in 1985 for quiescent systems [47, 48], which has also been found to hold under steady homogeneous flow [49]. For states close to the glass transition at ϕ_c, the decay of shear stress fluctuations at intermediate times is asymptotically given by

$$\begin{aligned} G(t, t_1, \mathbf{q}; [\dot\gamma]) &= G^c_\infty(q) \\ &+ H(\mathbf{q}) \Omega^a \, \mathcal{G}(t\Omega/\tau_0, (\phi - \phi_c)/(\phi_c \Omega^{2a}), \dot\gamma \tau_0 / \Omega^{(1+a)}) \\ &+ \mathcal{O}(\Omega^{2a}). \end{aligned} \tag{6}$$

The dominant term $G^c_\infty(q)$ is the frozen-in elasticity right at MCT's glass transition point. It is seen at intermediate times in $G_q(t)$ for closeby fluid states. It becomes the plateau shear modulus G^c_∞ at zero wavevector. The stability of the elastic structure is determined by the corrections to $G^c_\infty(q)$. Ω denotes a small scale and equation (6) holds for $\Omega \to 0$. The dominating correction contains the universal critical dynamics $\mathcal{G}$ of MCT; the exponent a is the critical exponent which takes the value $a = 0.32$ in a system of hard disks [50]. In quiescent glass states, viz. for $\dot\gamma = 0$ and $\phi > \phi_c$, elastic stresses are stored infinitely long, $\mathcal{G}(t\Omega/\tau_0 \to \infty, x > 0, 0) \to \text{const.} > 0$. This predicts $G(t \to \infty) \to G_\infty(\phi) > G^c_\infty$ in glass. In fluid states, $\phi < \phi_c$, and under steady shear, $\dot\gamma > 0$, the correction initiates the decay of elastic stresses, $\mathcal{G}(t\Omega/\tau_0 \to \infty, x < 0, y \neq 0) \to -\infty$. The final decay of the stress auto-correlation functions to zero is described by the α-scaling law in quiescent fluids [18], $G(t) \to \hat{G}(t/\tau) = G^c_\infty(1 - (t/\tau)^b + \ldots)$, where the von Schweidler exponent b (with $b = 0.60$ for hard disks) explains the stretching of the α-scaling function $\hat{G}$. The shear driven decay also follows a scaling function, which describes decay on a time-scale determined by the inverse shear rate: $G(t) \to \tilde{G}(t\dot\gamma) = G^c_\infty(1 - ct|\dot\gamma| + \ldots)$ with constant $c > 0$ [49].

ITT-MCT thus predicts a well defined static shear modulus $G_\infty(\phi)$ close to the glass transition which can be observed by various rheological or other measurements. Testing this prediction using computer simulations, is the main aim of our work.

3. Methods

3.1. 2D EDBD silmations

A 2D binary mixture of hard disks undergoing Brownian motion is simulated using an event-driven algorithm [28, 51, 52]. A quadratic simulation box containing a 50:50 mixture of hard disks with diameters $d_s = 1$ and $d_b = 1.4$ with periodic boundary conditions is employed. In a two-dimensional glass state finite size effects may appear [53–55], therefore the particle number N was varied between $N = 1000$ and 32 000. In an earlier work we showed that structural quantities in our system, if corrected by subtraction of the contributions from long wavelength density fluctuations, show weak finite size effects [32]. Apart from one exception for very high densities discussed below, no dependencies on system size could be resolved for the functions investigated in the following and a standard system with $N = 1000$ disks was chosen. To avoid aging dependencies the system is driven into a well-aged state employing Newtonian dynamics for a time corresponding to $25 \times 10^3 \tau_0$ with $\tau_0 = d_s^2/D_0$ the Brownian diffusion time set by the diffusion constant. (The mapping to the actual Brownian dynamics simulation (performed afterwards) is done by considering the final or α- relaxation times.) The shown data is based on at least 300 and up to 700 independent single runs for each packing fraction, shear rate or time interval, where the stress correlation functions were sampled for times up to $t = 5 \times 10^3 \tau_0$. The tested packing fractions, defined by the ratio of the area occupied by the disks to the total area, vary between $\phi = 0.7700$ and $\phi = 0.8100$. A fine grid with step width $\Delta\phi = 2.5 \times 10^{-3}$ is chosen in order to get an accurate estimate of the glass transition point which elsewhere was estimated at $\phi_c \approx 0.796$ [29].

3.1.1. The stress tensor. A general macroscopic expression for the stress tensor comes from the continuity equation of momentum flux in the system [56, 57]

$$\sigma_{\alpha\beta} = \frac{1}{V}\left(\sum_i (v_i - u_i)_\alpha (v_i - u_i)_\beta + \sum_{ij} (f_{ij})_\alpha (r_{ij})_\beta\right), \tag{7}$$

where $\mathbf{u}$ denotes the coarse-grained local velocity and f_{ij} the interparticle force associated with a pair potential. This expression represents the macroscopic stress, viz. a spatial average, which is legit for a spatially homogeneous structure. The first term on the right hand side represents the *kinetic* part, which is diagonal in the systems we investigate and linked to the thermal energy by the equipartition theorem. The thermostat employed keeps this contribution constant and we will not pay particular attention to it in the following. The second term gives the *potential* part and contains the contributions of the particle interactions.

Technically the hard body potential is infinite at contact of the particles and zero otherwise. The interparticle force for a system with impulsive interaction is best described with the help of the Dirac delta function

$$\mathbf{f}_{ij}(t) = \Delta\mathbf{p}_{ij}\delta(t - \tau_c), \tag{8}$$

the force is only non-zero at time τ_c of a collision, where $\Delta\mathbf{p}_{ij} = m_i\mathbf{r}_i - m_j\mathbf{r}_j$ denotes the exchange in momentum between the partners i and j of an elastic collision with mass m and velocity $\mathbf{r}$. This renders equation (7) in its current form unpractical. The appropriate modification is a replacement of the expression by its impulsive limit by integration over a short time interval Δt leading to [58]

$$\sigma_{\alpha\beta} = \frac{1}{\Delta t V}\sum_{\text{coll.}} \Delta p_\alpha(\tau_c)\Delta r_\beta(\tau_c), \tag{9}$$

where the sum runs over all binary collisions taking place in the volume V within the short measurement period of length Δt. The relative distance between the two particle centers at collision is denoted as $\Delta\mathbf{r}$. For reasonable results we demand the stress to be constant or vary slowly within the measurement interval Δt.

3.2. Method I: Shear modulus from stress fluctuations

The first approach to quantify the rigidity goes back to a method to determine transport coefficients that is almost as old as MD simulations itself. In 1970 Alder *et al* [59] used the mean squared integrated stress $\langle(\int_0^t \mathrm{d}s\sigma_{xy}(s))^2\rangle$ to determine the time dependent shear modulus $G(t)$. It can be obtained by taking two derivatives with respect to time t, using time translational invariance of correlation functions in equilibrium, and equation (9) for hard disks. The result is:

$$G(t) = \frac{1}{2Vk_\mathrm{B}T}\frac{\mathrm{d}^2}{\mathrm{d}t^2}\left\langle\left(\sum_{\tau_c\in[0,t]} \Delta p_x(\tau_c)\Delta r_y(\tau_c)\right)^2\right\rangle, \tag{10}$$

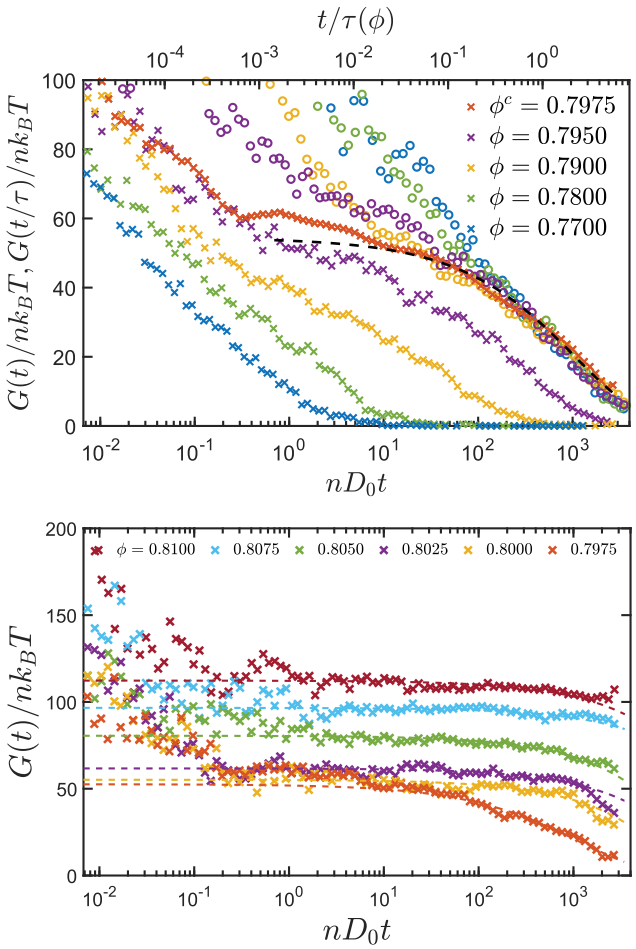

Figure 1. Shear stress auto-correlation function $G(t)$ (crosses) in equilibrium for different packing fractions ϕ in the supercooled liquid (upper panel; $\phi < \phi_c$) and glass (lower panel; $\phi > \phi_c$); from the α-scaling we estimate $\phi_c \approx 0.7975$. Circles show the scaled stress correlation functions falling on a master curve that is described by a Kohlrausch law $G_\infty \exp[-(t\tau(\phi^c)/\tau(\phi))^\beta]$ for $G_\infty = 54.4nk_\mathrm{B}T$, $\tau(0.7975) = 1554\tau_0$ and $\beta = 0.60$ (black dashed line); see the upper x-axis for the rescaled times. In the glass a fit $G(t) = G_\infty - c\sqrt{t}$ is added (dashed lines).

representing an approach that is compatible with the minimum image convention required by the periodic boundary conditions [60, 61]. With equation (10) the shear modulus $G(t)$ is sampled by the mean square of the summed oriented momentum transfer of all collisions within a time span [0,t]. The method was employed on time intervals of exponentially growing length, and the time derivatives were carried out numerically using differential quotients. An 11-point running average was performed on the resulting data.

Figure 1 shows the two step relaxation process of $G(t)$ in the liquid and the decay onto a long time plateau in the glass, which shows comparable features as simulation data from the literature [9, 10, 12, 13, 62–64]. For packing fractions $\phi < \phi_c = 0.7975$ the α-relaxation with its characteristic decay time $\tau(\phi)$ is resolved. This indicates the viscous nature of the supercooled liquid. The timescale of the structural relaxation τ obtained from the incoherent density correlation

function Φ_q presented in an earlier work [31] shows the same density dependence but is slightly larger than the stress relaxation time. The α-relaxation superposition principle allows to shift the final relaxation of the time dependent shear modulus for all densities onto a master curve. See the open circles in figure 1 and upper x-axis; the shifted times τ are given in the inset of figure 5 below. The scaling function is described by a stretched exponential $G(t,\phi) = G^c_\infty \exp[-t'^\beta_\phi]$, a so-called Kohlrausch law, with rescaled time $t'_\phi = t\tau(\phi^c)/\tau(\phi)$. We take the exponent $\beta = 0.6$ from a MCT calculation of hard disks [50] and fit the critical shear modulus, which gives $G^c_\infty = 54.4 n k_B T$. The height of this intermediate plateau governs the elastic response to rapid shear deformations in supercooled liquids close to the glass transition point. The scaling breaks down for values $\phi \geqslant \phi_c$, viz. for densities in the glass, because the plateau value $G_\infty(\phi)$ grows larger than G^c_∞ monotonically with $\phi - \phi_c$. While a fast-decay at $t \lesssim \tau_0$ is still observed, the final decay of the stress correlations shifts to the end of the simulation window when crossing the transition point. For an ideal glass transition as predicted by MCT [18], the plateau value G_∞ holds out to infinite time for $\phi \geqslant \phi_c$, while in experiments and simulations the stress relaxation often simply is shifted to times too large to be observed. Also in our case, the observed plateau is not stable and a small decay can be observed, which can be approximated by $G(t) = G_\infty - c\sqrt{t}$.

Figure 1 shows that the MCT predictions concerning G_∞ can be supported by the simulation data. Yet, using the superposition principle of the α-process is crucial for determining an accurate estimate of the glass transition density because of the relaxation processes present in glass states but not contained in MCT. Also the limited time window accessible by simulations prevents fitting the plateau value G_∞ without ambiguity in fluid states.

3.3. Method II: Shear modulus from displacement fluctuations

Klix *et al* [42, 45] used the second method presented above, to obtain microscopic expressions for the elastic shear and bulk modulus from the wave-vector dependent dispersion relations in amorphous solids. This approach was motivated by a technique to determine the dynamic matrix in a colloidal crystal in two dimensions by measurement of the spatial correlations via video microscopy [46]. The displacement field is defined relative to the time averages of the particle trajectories, which serves as the equivalents of lattice sites of a regular crystal. A particle's mean position $\bar{\mathbf{r}}_i$ is calculated by an average over a time Δt where $\tau_0 \ll \Delta t < \tau$, such that only the glassy part of the dynamics of the suspension is taken into account. The displacement of particle i is then defined as $\mathbf{u}_i(t) = \mathbf{r}_i(t) - \bar{\mathbf{r}}_i$, with $\mathbf{r}_i(t)$ its position at time t. The resulting collective displacement field is obtained from

$$\mathbf{u}_\mathbf{q}(t) = \frac{1}{\sqrt{N}} \sum_{i=1}^{N} e^{i\mathbf{q}\bar{\mathbf{r}}_i} \mathbf{u}_i(t). \tag{11}$$

This expression can be used in order to evaluate the displacement variance entering equation (5), and thereby to obtain the dispersion relations whose limit for small wavevectors gives the shear modulus $G_\infty = \mu$ and longitudinal modulus $G^{\|}_\infty = 2\mu + \lambda$, employing the familiar Lamé-notation. The elastic constants can be extracted from the longitudinal and transverse displacements $\mathbf{u}^{\|}(\mathbf{q})$ and $\mathbf{u}^{\perp}(\mathbf{q})$ by a quadratic fit for small wavevectors to the dispersion relations; we use $qd_s \leqslant 0.6$ and that the system is 2D:

$$\langle u^{\perp *}(\mathbf{q}) u^{\perp}(\mathbf{q})\rangle^{-1}_{\text{glass}} = \frac{\lambda_\perp(q)}{k_B T} \to q^2 \frac{G_\infty}{n k_B T} \quad \text{for } q \to 0 \tag{12}$$

$$\langle u^{\|*}(\mathbf{q}) u^{\|}(\mathbf{q})\rangle^{-1}_{\text{glass}} = \frac{\lambda_\|(q)}{k_B T} \to q^2 \frac{G^{\|}_\infty}{n k_B T} \quad \text{for } q \to 0. \tag{13}$$

As the displacement fluctuations are ergodic in this restricted phase space, $\langle\cdot\rangle_{\text{glass}}$ includes time averaging over a time interval of length $\Delta t < \tau$ using 10^4 configurational snapshots. Further an average over simulation runs and, as the systems investigated are isotropic, over directions in reciprocal space are performed. For this equation (11) was evaluated on a quadratic grid in q-space with lattice constant $\Delta q d_s = 0.17$.

Figure 2 shows the dispersion relations at two different packing fractions, one in the glass and one in the supercooled liquid. As predicted by equation (12) and (13) a quadratic dependence on q in the small wave vector limit is found indicating the solidity of the system during the tested time interval. From the quadratic fits, an effective stiffness $G_{\text{samp}}(\Delta t)$ is obtained. Measured data are very sensitive to the length of the time interval Δt over which positional data is collected [17]. While the precise functional form of the sampled stiffness $G_{\text{samp}}(\Delta t)$ cannot be related to the time-dependent shear modulus $G(\Delta t)$, we find that both track each other [65]. For short times $\Delta t \approx \tau_0$ the initial decay caused by short time diffusion is sampled leading to high values of $G_{\text{samp}}(\Delta t)$ for the glassy and fluid systems. These values embody the stiffening that is also seen in $G(t)$ for short times, equivalently in the linear response moduli for high frequencies [66, 67]. In glass, for larger sampling intervals this value saturates at $\lim_{\Delta t\to\infty} G_{\text{samp}}(\Delta t) = G_\infty$, in agreement with equation (12). In fluid states, at larger times (or lower frequencies) comparable to the system's α- relaxation time τ viscous flow due to the fluid structural rearrangements sets in. In this case the measurement time interval contains both short-time and long-time processes, but due to the equidistant sampling times of the configuration snapshots the latter dominate. Accordingly for densities below the critical value ϕ_c the dispersion relations flatten out and smaller and smaller $G_{\text{samp}}(\Delta t)$ are recorded for increasing Δt. This behavior allows for a rather strict distinction between glassy and fluid states. The values for the longitudinal moduli exceed the transversal ones clearly, it is $G^{\|}_\infty \approx 7 G_\infty$. In comparison to methods relying on the measurement of stresses and thus collision statistics, the dispersion relations determined by the displacement field profit from the good statistics from positional data. Consequently the noise

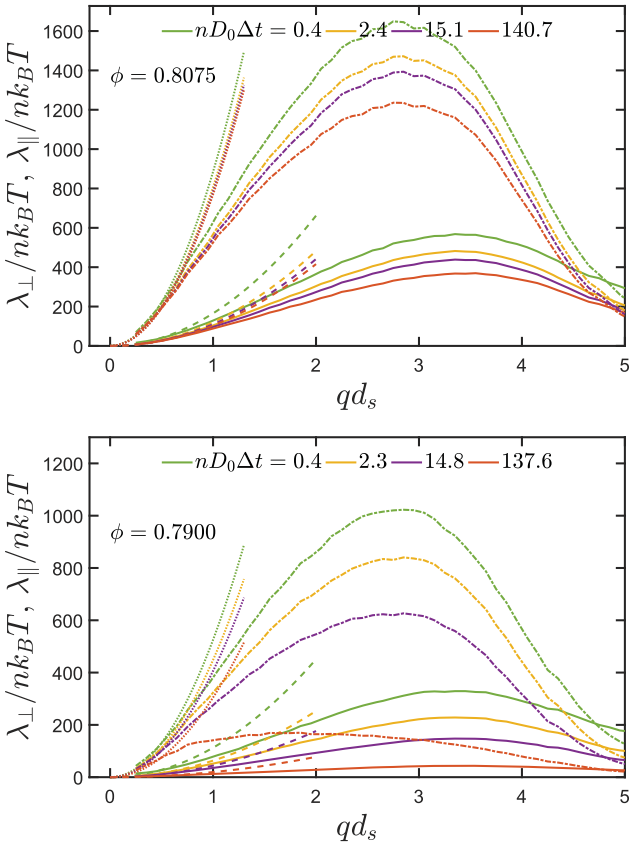

Figure 2. Transverse dispersion relation $\lambda_\perp(q)$ (solid lines) and parallel dispersion relation $\lambda_\parallel(q)$ (dashed-dotted lines) for the glass (upper panel, $\phi = 0.8075$) and supercooled liquid (lower panel, $\phi = 0.7900$) for varying sampling times Δt given in the legends. Quadratic fits (dashed lines, dotted lines) are added in the small wave vector limit yielding estimates of $G_{\text{samp}}(\Delta t)$; see the main text for their discussion.

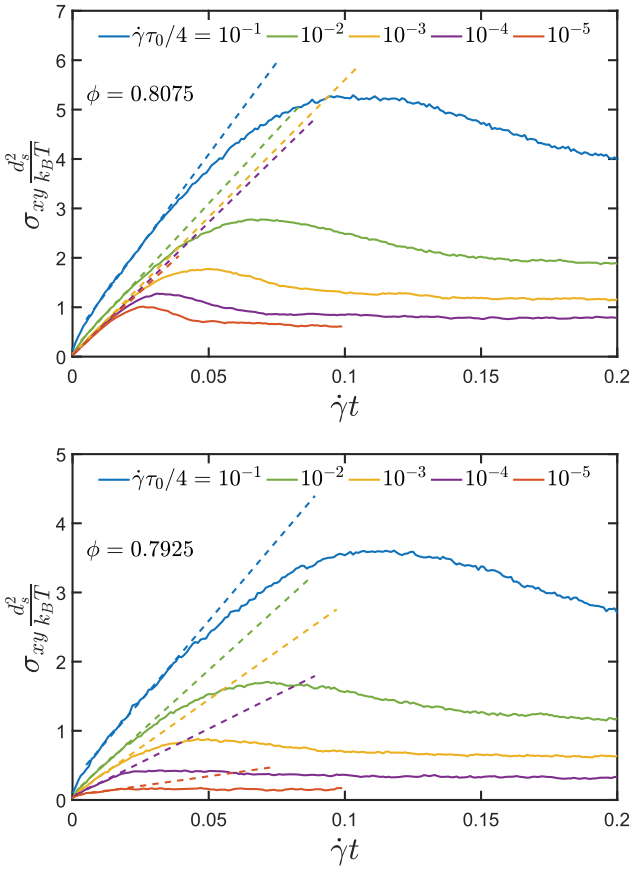

Figure 3. Stress–strain relation for the transient regime of startup of shear flow for the glass (upper panel, $\phi = 0.8075$) and supercooled liquid (lower panel, $\phi = 0.7925$) for varying shear rates $\dot\gamma$ given in the legends. Dashed lines show the linear fits $G_{\text{lin}}(1/\dot\gamma)\gamma + C$ at the strain interval of elastic response at strain $\dot\gamma t \approx 10^{-2}$. High (low) shear rates $\dot\gamma$ correspond to short (long) times t; see details in the main text. Again $G_{\text{lin}}(1/\dot\gamma)$ asymptotically saturates in the glass, now for $\dot\gamma \to 0$, while it decays to zero in the fluid.

level of the shown curves is very low and allows for an accurate determination of the moduli.

3.4. Method III: Shear modulus from stress–strain relations under startup shear flow

In the following we use a flow-protocol

$$\dot\gamma(t) = \begin{cases} 0 & t < 0 \\ \dot\gamma & t \geqslant 0 \end{cases} \tag{14}$$

to examine the effect of a finite shear rate on the shear stress in the system. At times $t < 0$ the system is in an unperturbed, well aged state with vanishing shear stress $\langle\sigma_{xy}(t)\rangle = 0$. From $t = 0$ on the system undergoes shear with a constant and spatially homogeneous shear rate $\dot\gamma$ [28]. For $t > 0$ during startup flow the transient stresses as function of the accumulated strain $\gamma = \dot\gamma t$ are given by

$$\sigma_{xy}(t,\dot\gamma) = \int_0^t \dot\gamma G(t',\dot\gamma)\mathrm{d}t' = \frac{1}{\Delta t V}\sum_{\text{coll.}} \Delta p_x(\tau_c)\Delta r_y(\tau_c), \tag{15}$$

where again the sum runs over all collisions within a small time window Δt around t (see section 3.1.1) and $G(t,\dot\gamma)$ denotes the shear rate dependent stress kernel of equation (4).

Figure 3 shows the transient stress σ_{xy} as function of the accumulated strain $\dot\gamma t$ for a glassy system at packing fraction $\phi = 0.8075$ and a fluid one at $\phi = 0.7925$. In the initial response for strains $\gamma \lesssim 0.02$, the suspensions behave like a solid and the shear stress grows linearly with strain, just like Hooke's law describes the linear response of elastic bodies as $\sigma_{xy} = G_{\text{lin}}\gamma$. Obviously this also holds in fluids for short times. Then the system transiently stores an increasing amount of elastic energy until it yields around the overshoot at $\gamma \approx 0.07$. From there, the shear stress decreases monotonically to the steady stress level $\sigma_{xy}^{\text{stat}}$ associated with a stationary state that is reached for $\gamma \gtrsim 1$; for comparable results see [68–70]. In the regime of elastic response we obtain $G(t)$ from a linear fit $f_{\dot\gamma}(\gamma) = G(t)\gamma + C$ to the stress data. Shear rates $\dot\gamma$ corresponding to Peclet numbers $\dot\gamma\tau_0 \in [4\times10^{-5}, 4\times10^{-1}]$ have been applied and C is negligible for $\dot\gamma\tau_0$ below 10^{-2}. The stress versus accumulated strain curves depend rather weakly on the applied strain rates. The linear response regime and the stress overshoot region is shifted to smaller strain regions for lower shear rates. To fix the $\dot\gamma$-dependent interval of elastic response, we considered the time intervat $[t_0, t_1] = [0.05t^*_{\dot\gamma}, 0.3t^*_{\dot\gamma}]$, where $t^*_{\dot\gamma}$ denotes the time at the stress maximum. Accordingly for

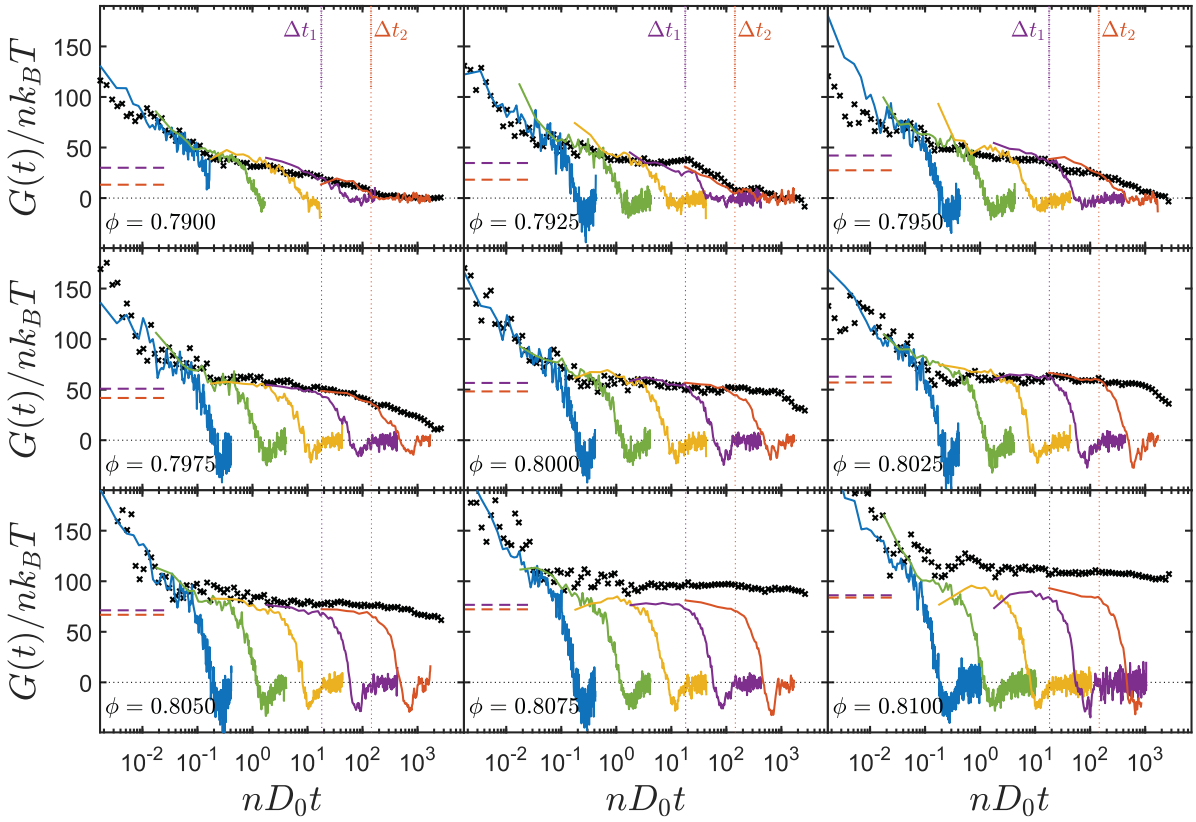

Figure 4. Comparison between the estimates for the time-dependent shear modulus $G(t)$ for quiescent (black crosses) and sheared systems for shear rates $\dot{\gamma}\tau_0 = 4 \times 10^{-1}$(blue), 4×10^{-2} (green), 4×10^{-3} (yellow), 4×10^{-4} (purple), 4×10^{-5} (orange) and varying densities as labeled. The purple and orange dashed horizontal lines indicate the value for G_∞ from displacement fluctuations determined for $\Delta t_1 = 22\tau_0$ and $\Delta t_1 = 203\tau_0$; these time intervals are marked by vertical dotted lines. In the glass for $\phi < 0.805$ the obtained plateau values are in very good agreement, while deep in the glass for $\phi \geqslant 0.805$ Method I overestimates $G(t)$ compared to Methods II and III.

decreasing shear rate the value of t_1 increases nearly with $1/\dot{\gamma}$. Therefore we are able to sample $G_{\text{lin}}(1/\dot{\gamma})$ over 5 decades by varying $\dot{\gamma}$ over 5 decades. For high $\dot{\gamma}$ the shear start-up interferes with the initial short-time motion resulting in high values. In the glass the values of the linear slopes saturate for decreasing shear rates, $G_{\text{lin}}(1/\dot{\gamma} \to \infty) \to G_\infty$, and yield the static shear modulus. The slow approach is in line with the very slow decay to the intermediate plateau seen in the time-dependent shear moduli. In the liquid for small shear rates corresponding to large times, the effective linear shear modulus $G_{\text{lin}}(1/\dot{\gamma})$ has almost completely decayed to zero. More precisely for $\dot{\gamma}\tau_0 \lesssim 10^{-4}$ the chosen time window exceeds the structural relaxation time and the response becomes viscous.

4. Results and discussion

The methods described above are capable of quantifying the level of rigidity in terms of the time dependent shear modulus $G(t)$ over five decades in time. Using identical initial positional configurations of the simulation runs, we are able to compare the findings of the different measurements unambiguously. Method III is based on the fact, that in the strain window of linear response the $\dot{\gamma}$-dependent shear modulus $G(t,\dot{\gamma})$ coincides with the shear modulus $G(t)$ at rest, see section 2.1. From equation (15), the nonlinear shear modulus is $G(t,\dot{\gamma}) = \dot{\gamma}^{-1}\partial_t\sigma_{xy}(t,\dot{\gamma})$. The derivative is numerically evaluated using a five point rule. Method I provides $G(t)$ directly, see equation (2). The two quantities are shown in figure 4 for packing fractions close to the glass transition point. Additionally, the estimates of $G_\infty(\phi)$ from the displacement fluctuations (Method II) for two different sampling windows Δt are included as horizontal bars.

Figure 4 is the central result of our study. Both the quiescent and the sheared time-dependent modulus exhibit a fast short time relaxation, which is $\dot{\gamma}$-independent within the scatter of the data. For longer times, the linear time-dependent moduli exhibit the transient plateau given by $G_\infty(\phi)$ for time ranges limited by the α-relaxation time τ. The nonlinear moduli also relax onto the plateau $G_\infty(\phi)$, which is transient for the sheared system and corresponds to the linear growth of the shear stress during elastic response. After that $G(t,\dot{\gamma})$ decays on a time $\tau_{\dot{\gamma}} \sim \dot{\gamma}^{-1}$ roughly proportional to the inverse shear rate. This shear rate dependence is equivalent to the observation of the peak position in the stress–strain relations that varies only slightly with $\dot{\gamma}$. Further this shear stress overshoot translates into an undershoot in the shear moduli. For large times the function vanishes as soon as a stationary state with a stress tensor that is constant in time is reached.

For densities $\phi \leqslant 0.805$ the quiescent modulus $G(t)$ can be reassembled by putting together the transient plateaus of the sheared modulus $G(t,\dot{\gamma})$ for the various shear rates. For densities not too high, a close agreement between the moduli

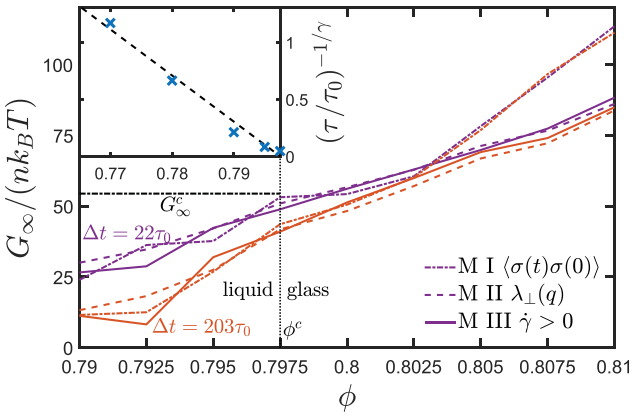

Figure 5. Density dependence of the plateau shear modulus G_∞ as worked out using the 3 methods: for two long times $t = 22\tau_0$ (purple) and $t = 203\tau_0$ (orange) (Method I), for the two largest measurement intervals of length $\Delta t = 22\tau_0$ (purple) and $\Delta t = 203\tau_0$ (orange) (Method II), and for the two corresponding smallest shear rates $\dot\gamma\tau_0 = 4 \times 10^{-4}$ (purple) and $\dot\gamma\tau_0 = 4 \times 10^{-5}$ (orange) (Method III). Also, the critical shear modulus G^c_∞ from the α-scaling in the fluid is included. The inset shows the divergence of the relaxation time τ with $\gamma = 2.38$ predicted from theory [50], where the dashed line indicates a fit $y = 40.5(\phi^c - \phi)$ to the expected linear behavior.

from Methods I and III is found, both in the supercooled liquid as well as in the glass. The static moduli $G_\infty(\phi)$ from Method II are added in figure 4 using two different values Δt of the sampling window. The Δt values are indicated by vertical lines. As discussed, the estimated static moduli $G_\infty^{\text{method II}}(\phi)$ agree if the time window Δt is chosen such that the sampling is dominated by the elastic region, where $G(t) \approx G_\infty$. For low densities, choosing too large Δt gives strongly differing estimates, because the displacement fluctuations are falsified by structural motion. For packing fraction above $\phi \geqslant 0.80$, the static moduli $G_\infty(\phi)$ from Methods II and III agree as expected from the assumptions entering both methods. Combining all three methods thus provides the static moduli for the complete range of densities around the glass transition value $\phi_c \approx 0.7975$, which was estimated from the α-scaling property. This reinforces the validity of the applied methods and the underlying relations for the shear modulus predicted by MCT. The short time response for times $t < \tau_0$ cannot be determined reliably in our simulations, owing particularly to high noise levels because of short sampling times and high Pèclet numbers (Method III) corresponding to strong external driving.

For packing fractions $\phi \geqslant 0.805$, Method I overestimates the plateau value, predicted consistently by the other two methods, by up to 20%. This deviation was observed for several system sizes from $N = 500$ up to 64 000 particles (not shown), where an additional spreading of the plateau values was found showing no clear trend in the size dependence. The other two methods found no dependence on the particle number N. Further in a careful analysis no signs of aging effects could be found and regarding the distribution of single runs no statistical outliers causing this behavior were detected. We therefore judge Method I to be untrustworthy for states deep in the glass. In [42], the same system was investigated by comparable simulations and different results were obtained for Method I. We found that the differences are based on inaccurate processing of the positional data in the simulations of [42], and judge our data to be correct.

Figure 5 shows the ϕ-dependence of G_∞ as obtained using all three methods. A small step width of $\Delta\phi = 2.5 \times 10^{-3}$ allows to resolve the rapid but continuous increase of $G_\infty(\phi)$ in a narrow region around the glass transition. For all methods, data using the two very long measurement times t (Method I), measurement intervals Δt (Method II), or inverse shear rates $1/\dot\gamma$ (Method III), are shown with time spans considerably larger than τ_0. For packing fractions in the fluid the α- relaxation has already set in at the times employed and all methods obtain values smaller than the constant plateau modulus G^c_∞ predicted by MCT. It can only reliably be determined from the α-scaling of the linear moduli for different ϕ (see upper panel in figure 1), or from the $\dot\gamma$-scaling of the nonlinear moduli visible in figure 4. The thus obtained estimates of the α- relaxation times τ, which should algebraically diverge according to MCT, $\tau \sim (\phi_c - \phi)^{-\gamma}$ [18] with exponent $\gamma \approx 2.38$ for monodisperse hard disks [50], support the estimate of ϕ_c; see the inset of figure 5. In the glass, the agreement between the values determined using the different methods is satisfactory except for the the deviation of the plateau value in $G(t)$ (Method I) deep in the glass.

5. Conclusions

We presented the simulational results of the sampling of the time dependent shear modulus of a two dimensional Brownian mixture of hard disks close to its glass transition. We showed that the shear modulus $G_\infty(\phi)$ as predicted by mode coupling theory is accessible from the plateau value of the stress correlation function, the suspension's dispersion relations, and the linear stress–strain relations during startup of simple shear flow. Controlling the packing fraction, we approached the glass transition from the fluid regime and determined a finite, constant shear modulus $G^c_\infty = G_\infty(\phi_c)$. Upon further densification in the glass, this value grows, representing a stiffening of the solid system. Verified by consistent results from all applied measurements, we presented a procedure to unambiguously determine the glass transition point according to MCT which is in line with existing experimental works [71]. Deep in the glass we found deviations of G_∞ obtained by sampling the stress auto correlation function from the values obtained by the two other methods. The plateau values of the stress correlation functions are above the values obtained from the response to external shear or from the dispersion relations. This discrepancy is presently not understood.

Acknowledgments

The authors thank J Baschnagel, P Keim, F Varnik, Th Voigtmann and F Weyßer for helpful discussions regarding the simulations and the interpretation of the data. SF was supported in part by German Research Foundation FOR 1394, Project P3.

ORCID iDs

S Fritschi https://orcid.org/0000-0002-2798-8413

References

[1] Mewis J and Wagner N J 2012 *Colloidal Suspension Rheology* (Cambridge: Cambridge University Press)
[2] Hunter G L and Weeks E R 2012 The physics of the colloidal glass transition *Rep. Prog. Phys.* **75** 066501
[3] Pusey P N and van Megen W 1986 Phase behaviour of concentrated suspensions of nearly hard colloidal spheres *Nature* **320** 340–2
[4] Mason T G and Weitz D A 1995 Optical measurements of frequency-dependent linear viscoelastic moduli of complex fluids *Phys. Rev. Lett.* **74** 1250–3
[5] Siebenbürger M, Fuchs M and Ballauff M 2012 *Soft Matter* **8** 4025–43
[6] Dhont J K G 1996 *An Introduction to Dynamics of Colloids* (Amsterdam: Elsevier)
[7] Tokuyama M and Oppenheim I 1994 Dynamics of hard-sphere suspensions *Phys. Rev.* E **50** R16–9
[8] Szamel G and Flenner E 2011 Emergence of long-range correlations and rigidity at the dynamic glass transition *Phys. Rev. Lett.* **107** 105505
[9] Abraham S and Harrowell P 2012 The origin of persistent shear stress in supercooled liquids *J. Chem. Phys.* **137** 014506
[10] Wittmer J P, Xu H, Polińska P, Weysser F and Baschnagel J 2013 Shear modulus of simulated glass-forming model systems: Effects of boundary condition, temperature, and sampling time *J. Chem. Phys.* **138** 12A533
[11] Lemaître A 2014 Structural relaxation is a scale-free process *Phys. Rev. Lett.* **113** 245702
[12] Flenner E and Szamel G 2015 Long-range spatial correlations of particle displacements and the emergence of elasticity *Phys. Rev. Lett.* **114** 025501
[13] Wittmer J P, Xu H and Baschnagel J 2015 Shear-stress relaxation and ensemble transformation of shear-stress autocorrelation functions *Phys. Rev.* E **91** 022107
[14] Saw S and Harrowell P 2016 Rigidity in condensed matter and its origin in configurational constraint *Phys. Rev. Lett.* **116** 137801
[15] Chowdhury S, Abraham S, Hudson T and Harrowell P 2016 Long range stress correlations in the inherent structures of liquids at rest *J. Chem. Phys.* **144** 124508
[16] Kriuchevskyi I, Wittmer J P, Benzerara O, Meyer H and Baschnagel J 2017 Numerical determination of shear stress relaxation modulus of polymer glasses *Eur. Phys. J.* E **40** 43
[17] Kriuchevskyi I, Wittmer J P, Meyer H and Baschnagel J 2017 Shear modulus and shear-stress fluctuations in polymer glasses *Phys. Rev. Lett.* **119** 147802
[18] Götze W 2009 *Complex Dynamics of Glass-Forming Liquids, a Mode-Coupling Theory* (Oxford: Oxford University Press)
[19] Leutheusser E 1984 Dynamical model of the liquid-glass transition *Phys. Rev.* A **29** 2765
[20] Chong S, Moreno A J, Sciortino F and Kob W 2005 Evidence for the weak steric hindrance scenario in the supercooled-state reorientational dynamics *Phys. Rev. Lett.* **94** 215701
[21] Voigtmann T 2011 Multiple glasses in asymmetric binary hard spheres *Europhys. Lett.* **96** 36006
[22] Seyboldt R, Hajnal D, Weysser F and Fuchs M 2012 Shear moduli of two dimensional binary glasses *Soft Matter* **8** 4132–40
[23] Siebenbürger M, Fuchs M, Winter H and Ballauff M 2009 *J. Rheol.* **53** 707–26
[24] Brader J M, Cates M and Fuchs M 2008 First-principles constitutive equation for suspension rheology *Phys. Rev. Lett.* **101** 138301
[25] Brader J M, Cates M E and Fuchs M 2012 First-principles constitutive equation for suspension rheology *Phys. Rev.* E **86** 021403
[26] Amann C P, Siebenbürger M, Ballauff M and Fuchs M 2015 Nonlinear rheology of glass-forming colloidal dispersions: transient stress–strain relations from anisotropic mode coupling theory and thermosensitive microgels *J. Phys.: Condens. Matter* **27** 194121
[27] Crassous J J, Siebenbürger M, Ballauff M, Drechsler M, Hajnal D, Henrich O and Fuchs M 2008 *J. Chem. Phys.* **128** 204902
[28] Henrich O, Weysser F, Cates M E and Fuchs M 2009 Hard discs under steady shear: comparison of brownian dynamics simulations and mode coupling theory *Phil. Trans. R. Soc.* A **367** 5033–50
[29] Weysser F and Hajnal D 2011 Tests of mode-coupling theory in two dimensions *Phys. Rev.* E **83** 041503
[30] Fritschi S, Fuchs M and Voigtmann T 2014 Mode-coupling analysis of residual stresses in colloidal glasses *Soft Matter* **10** 4822–32
[31] Illing B, Fritschi S, Hajnal D, Klix C L, Keim P and Fuchs M 2016 Strain pattern in supercooled liquids *Phys. Rev. Lett.* **117** 208002
[32] Illing B, Fritschi S, Kaiser H, Klix C L, Maret G and Keim P 2017 Mermin-wagner fluctuations in 2d amorphous solids *Proc. Natl Acad. Sci.* **114** 1856–61
[33] Götze W 1999 *J. Phys.: Condens. Matter* **11** A1
[34] Voigtmann T 2014 Nonlinear glassy rheology *Curr. Opin. Colloid Interface Sci.* **19** 549
[35] Brader J M 2010 Nonlinear rheology of colloidal dispersions *J. Phys.: Condens. Matter* **22** 363101
[36] Cárdenas H, Frahsa F, Fritschi S, Nicolas A, Papenkort S, Voigtmann T and Fuchs M 2017 Nonlinear mechanical response of supercooled melts under applied forces *Eur. Phys. J. Spec. Top.* **226** 3039
[37] Varnik F and Henrich O 2006 Yield stress discontinuity in a simple glass *Phys. Rev.* B **73** 174209
[38] Ikeda A and Berthier L 2013 Yield stress in amorphous solids: a mode-coupling-theory analysis *Phys. Rev.* E **88** 052305
[39] Furukawa A and Tanaka H 2011 Direct evidence of heterogeneous mechanical relaxation in supercooled liquids *Phys. Rev.* E **84** 061503
[40] Nägele G and Bergenholtz J 1998 Linear viscoelasticity of colloidal mixtures *J. Chem. Phys.* **108** 9893–904
[41] Hansen J-P and McDonald I R 1986 *Theory of Simple Liquids* (London: Academic)
[42] Klix C, Ebert F, Weysser F, Fuchs M, Maret G and Keim P 2012 Glass elasticity from particle trajectories *Phys. Rev. Lett.* **109** 178301
[43] Maier M, Zippelius A and Fuchs M 2017 Emergence of long-ranged stress correlations at the liquid to glass transition *Phys. Rev. Lett.* in preparation (arXiv:1709.09962)
[44] Chattoraj J and Lemaître A 2013 Elastic signature of flow events in supercooled liquids under shear *Phys. Rev. Lett.* **111** 066001
[45] Fuchs M 2013 Elastic properties of colloidal solids with disorder ed C Bechinger *Physics of Complex Colloids: Proc. of the Int. School of Physics Enrico Fermi, Course 184 (Varenna on Lake Como, 3–13 July 2012) (Proc. of the Int. School of Physics 'Enrico Fermi'* vol 184) (Amsterdam: IOS Press) pp 75–94
[46] Keim P, Maret G, Herz U and von Grünberg H 2004 Harmonic lattice behavior of two-dimensional colloidal crystals *Phys. Rev. Lett.* **92** 215504
[47] Götze W 1985 Properties of the glass instability treated within a mode coupling theory *Z. Phys.* B **60** 195–203

[48] Franosch T, Fuchs M, Götze W, Mayr M R and Singh A P 1997 Asymptotic laws and preasymptotic correction formulas for the relaxation near glass-transition singularities *Phys. Rev.* E **55** 7153–76
[49] Fuchs M and Cates M E 2003 Schematic models for dynamic yielding of sheared colloidal glasses *Faraday Discuss.* **123** 267–86
[50] Bayer M, Brader J M, Ebert F, Fuchs M, Lange E, Maret G, Schilling R, Sperl M and Wittmer J P 2007 Dynamic glass transition in two dimensions *Phys. Rev.* E **76** 011508
[51] Scala A, Voigtmann Th and De Michele C 2007 Event-driven brownian dynamics for hard spheres *J. Chem. Phys.* **126** 134109
[52] Scala A 2012 Event-driven langevin simulations of hard spheres *Phys. Rev.* E **86** 026709
[53] Flenner E and Szamel G 2015 Fundamental differences between glassy dynamics in two and three dimensions *Nat. Commun.* **6** 7392
[54] Vivek S, Kelleher C P, Chaikin P M and Weeks E R 2017 Long-wavelength fluctuations and the glass transition in two dimensions and three dimensions *Proc. Natl Acad. Sci.* **114** 1850–5
[55] Shiba H, Yamada Y, Kawasaki T and Kim K 2016 Unveiling dimensionality dependence of glassy dynamics: 2d infinite fluctuation eclipses inherent structural relaxation *Phys. Rev. Lett.* **117** 245701
[56] Irving J H and Kirkwood J G 1950 The statistical mechanical theory of transport processes. IV. The equations of hydrodynamics *J. Chem. Phys.* **18** 817
[57] Rapaport D C 2004 *The Art of Molecular Dynamics Simulation* (New York: Cambridge University Press)
[58] Erpenbeck J J and Wood W W 1977 *Molecular Dynamics Techniques for Hard-Core Systems* (New York: Plenum)
[59] Alder B J, Gass D M and Wainwright T E 1970 Studies in molecular dynamics. VIII. The transport coefficients for a hard-sphere fluid *J. Chem. Phys.* **53** 3813–26
[60] Allen M P, Brown D and Masters A J 1994 Comment on use of the McQuarrie equation for the computation of shear viscosity via equilibrium molecular dynamics *Phys. Rev.* E **49** 2488
[61] Allen M P 1994 Comment on relationship between McQuarrie and Helfand equations for the determination of shear viscosity from equilibrium molecular dynamics *Phys. Rev.* E **50** 3277
[62] Xu H, Wittmer J P, Polińska P and Baschnagel J 2012 Impulsive correction to the elastic moduli obtained using the stress-fluctuation formalism in systems with truncated pair potential *Phys. Rev.* E **86** 046705
[63] Schnell B, Meyer H, Fond C, Wittmer J P and Baschnagel J 2011 Simulated glass-forming polymer melts: glass transition temperature and elastic constants of the glassy state *Euro. Phys. J.* E **34** 97
[64] Puertas A M, Zaccarelli E and Sciortino F 2005 Viscoelastic properties of attractive and repulsive colloidal glasses *J. Phys.: Condens. Matter* **17** L271
[65] Fritschi S 2017 Event-driven Brownian dynamics simulations of two-dimensional fluids far from equilibrium *PhD Thesis* Universität Konstanz in preparation
[66] Jeong H Y 1987 Frequency-dependent shear modulus of glycerol near the glass transition *Phys. Rev.* A **36** 766–73
[67] Brader J, Siebenbürger M, Ballauff M, Reinheimer K, Wilhelm M, Frey S J, Weysser F and Fuchs M 2010 Nonlinear response of dense colloidal suspensions under oscillatory shear: mode-coupling theory and fourier transform rheology experiments *Phys. Rev.* E **82** 061401
[68] Amann C P, Siebenbürger M, Krüger M, Weysser F, Ballauff M and Fuchs M 2013 Overshoots in stress–strain curves: colloid experiments and schematic mode coupling theory *J. Rheol.* **57** 149–75
[69] Koumakis N, Laurati M, Egelhaaf S U, Brady J F and Petekidis G 2012 Yielding of hard-sphere glasses during start-up shear *Phys. Rev. Lett.* **108** 098303
[70] Varnik F, Bocquet L and Barrat J-L 2004 A study of the static yield stress in a binary Lennard-Jones glass *J. Chem. Phys.* **120** 2788–801
[71] Klix C L, Maret G and Keim P 2015 Discontinuous shear modulus determies the glass transition temperature *Phys. Rev.* X **5** 041033